CORE
Metadata, citation and similar papers at core.ac.uk
Provided by Loughborough University Institutional Repository

Evaluating the cascading impacts of sea level rise and coastal flooding on emergency response spatial accessibility in Lower Manhattan, New York City

Jie Yin[1, 2, 3*], Dapeng Yu[4], Ning Lin[3], Robert L. Wilby[4]

1 Key Laboratory of Geographic Information Science (Ministry of Education), East China Normal University, China
2 School of Geographic Sciences, East China Normal University, China
3 Department of Civil and Environmental Engineering, Princeton University, US
4 Centre for Hydrological and Ecosystem Science, Department of Geography, Loughborough University, UK

Abstract: This paper describes a scenario-based approach for evaluating the cascading impacts of sea level rise (SLR) and coastal flooding on emergency responses. The analysis is applied to Lower Manhattan, New York City, considering FEMA's 100- and 500-year flood scenarios and New York City Panel on Climate Change (NPCC2)'s high-end SLR projections for the 2050s and 2080s, using the current situation as the baseline scenario. Service areas for different response timeframes (3-, 5- and 8-minute) and various traffic conditions are simulated for three major emergency responders (i.e. New York Police Department (NYPD), Fire Department, New York (FDNY) and Emergency Medical Service (EMS)) under normal and flood scenarios. The modelling suggests that coastal flooding together with SLR could result in proportionate but non-linear impacts on emergency services at the city scale, and the performance of operational responses is largely determined by the positioning of emergency facilities and the functioning of traffic networks. Overall, emergency service accessibility to the city is primarily determined by traffic flow speed. However, the situation is expected to be further aggravated during coastal flooding, with is set to increase in frequency and magnitude due to SLR.

Keywords: Emergency response; coastal flooding; sea level rise; Lower Manhattan

1 Introduction

Sea level rise (SLR) is among the most certain consequences of anthropogenic climate change, with significantly adverse effects on coastal settlements and ecosystems through permanent inundation of low-lying waterfront areas and by aggravating coastal flooding over a larger inland region (Hu and Deser, 2012; Nicholls and Cazenave, 2010). Tide gauge records show that global mean sea level rose by an average rate of 1.6 to 1.9 mm/year over the twentieth century (Hay et al., 2015), and CMIP5 climate models project a rise of 0.26 to 0.82 m in mean sea level rise by the end of 21st century (IPCC, 2012). Regional rates of sea level change vary from the global mean, due to local changes in oceanic circulation, variations in ocean temperature and salinity, vertical land movements, and static equilibrium processes (Mitrovica et al., 2001; Levermann et al., 2005; Kopp et al., 2014). For example, sea level has risen by 3 mm/year since 1900 in the vicinity of New York City (NYC) with only 60% of the observed SLR driven by climate-related factors and the remaining 40% caused by local factors (such as land subsidence). Climate model projections suggest a further rise of up to 1.9 m by 2100 (Peltier, 2004; Engelhart and Horton, 2012; Horton et al., 2015).

The effect of SLR on coastal flooding is well-documented globally. In the New York Harbor region SLR has significantly increased the frequency and/or intensity of storm tide flooding, with eight of the largest twenty extreme water levels occurring after 1990 (Talke et al., 2014). Hurricane Sandy generated the highest storm tide in the city's history and the most destructive flooding over NYC, resulting in considerable losses (45 deaths and more than $20 billion loss) and extensive indirect impacts (e.g. interruption of citywide infrastructure and public services) (NYC OEM, 2014). Towards the end of the 21st century, even if storm climatology does not change, the current 100-year flood for the city is projected to occur 2 to 4 times more often under the middle range of local NYC SLR estimates (Horton et al., 2015) and the current Sandy-like flood is projected to occur over 4 times more often (Lin et al., 2016) due to SLR. Hence, without further coastal adaptations, the city is expected to experience increasing flood risks under a changing climate (Aerts et al., 2014; Hallegatte et al., 2013).

In response to evolving coastal flooding, local governments are required to provide efficient risk management to meet legislative requirements (e.g. response time for high priority incidents) (Rosenzweig and Solecki, 2014). Emergency services are in the front-line of the operational response. In the United States, emergency responses (such as search, rescue and emergency medical services (EMS)) to hazards operating at local (city or community) scale are mostly provided by a division of the Police and/or Fire Departments with the responsibility to dispatch emergency resources to save lives and reduce damages as soon as possible during an event. During and after Hurricane Sandy, there was a 37-fold increase in water rescues compared to the normal conditions. The New York City Police Department (NYPD) and Fire Department of the City of New York (FDNY) rescued more than 2,200 people from the rising water of the storm and performed grid searches of more than 31,000 homes and businesses once floodwaters receded (NYC Mayor's Office, 2012).

There has been limited research into the cascading impacts of flood-induced road network failures on emergency service provisions in a changing climate. A few studies focus on the development and application of high resolution coastal flood models (e.g. Bates et al. 2005; Blumberg et al. 2015; Wang et al. 2014; Ramirez et al. 2016); others address the impacts of flooding on surface transportation system (e.g. Chang et al. 2010). For example, Gil & Steinbach (2008) evaluated the indirect consequences of flooding on an urban street network by removing flooded road sections from the transport system. Yin et al. (2016a) used a high resolution 2D inundation model and a flood depth-dependent measure (30 cm) to examine the accessibility losses of an intra-urban road network under various flood magnitudes. Identification of flood hotspots and extent of disrupted road network enables evaluation of impacts on emergency responders' performance. More recently, a framework for incorporating flood modelling with accessibility mapping for emergency responders has been developed by Coles et al. (2017), and demonstrated in the City of York with pluvial and fluvial events occurred in the city. Similarly, Green et al. (2017) evaluated the spatial coverage of emergency responders during pluvial and fluvial flood risks with various return periods for the City of Leicester, UK. Both studies focus on the accessibility of emergency responders to vulnerable populations (e.g. care homes) during flood events and within mandatory timeframes (8 minutes for Ambulance Service and 10 minutes for Fire & Rescue Service in the UK).

Although there is no federal or state standard for emergency response time in the U.S., some requirements do exist in different communities. For example, EMS is mandated by the NYC to meet an average 10-minute response time on emergency calls. According to 911 performance statistics collected for NYC[1] since November 2012, the majority of the End-to-End response time (including pickup, dispatch, processing and travel) was spent on traveling (3 to 9

[1] http://www.nyc.gov/html/911reporting/html/reports/end-to-end.shtml

minutes). During coastal flood emergencies, waterfront road networks can be affected by inundation, leading to significant travel delays (i.e. longer response times) and even widespread disruption of emergency services. The efficiency of coastal flood emergency response largely depends on the functioning of transport network in the coastal floodplain. For instance, storm surge associated with hurricane Sandy flooded large proportions of the coastal road network of NYC, especially in the Manhattan area, delaying emergency fire response in Queens (FEMA, 2012).

In this paper, we develop a scenario-based approach to quantify the impacts of SLR and coastal flooding on urban emergency response times using hydrodynamic modeling and GIS-based network analysis. Lower Manhattan (downtown and midtown, south of 57th Street), the Central Business District (CBD) of NYC, was used as a case study as it is highly vulnerable to coastal flooding induced by storm surge, which is expected to increase due to the change of storm climatology, in a magnitude comparable to the projected sea-level rise (SLR) (Lin et al., 2012). For example, the combined effects of storm climatology change and a 1-m SLR may result in the current NYC 100-year surge flooding to occur every 3-20 years and the 500-year flooding to occur every 25-240 years, by the end of the century (Lin et al., 2012). We begin by exploring the spatial-temporal characteristics of coastal flooding with rapid SLR over the coming decades. We then use the flood maps generated to investigate accessibility of the city by emergency services and to identify vulnerable facilities that lie within the inundated areas. Section 2 introduces the materials and methods, including data, coastal flood modeling and emergency service evaluation; Section 3 presents the results and discusses the key findings; finally, Section 4 provides the conclusions and offers suggestions for further research.

2 Materials and methods

2.1 Data and processing

2.1.1. Flood scenarios

Coastal flood scenarios were designed to evaluate the potential impacts of flooding on emergency service response. We apply FEMA's 100-year and 500-year coastal flood estimates for NYC to establish the current and baseline flood scenarios. Based on the frequency analysis undertaken by FEMA flood insurance study in 2012 (FEMA, 2012), the flood heights above NAVD 88 Datum for 1 in 100- and 500-year events along the NYC floodplain-sea boundary are used. To account for the effect of SLR, projected SLRs (see below) are linearly added to these baseline floods to create the flood scenarios for the 2050s and 2080s. Here we do not consider possible changes in the storm climatology in the future climate (Lin et al., 2012 and 2016).

2.1.2 Local sea level rise

In this study, we apply NPCC2's SLR projection for NYC, which were developed based on a seven-component approach (Horton et al., 2015), including relative ocean height, local fingerprint associated with the ocean's responses to ice mass loss, and land height change terms (NPCC2, 2013). The report is widely regarded as the most systematic study of SLR in NYC and has been officially adopted by local government in coastal resilience planning. Compared to other SLR studies (e.g. Kopp et al., 2014), the NPCC2's results show a wider range primarily due to the different sources of components considered, assumptions made and distributions assumed. To account for plausible yet extreme scenarios, high-end estimates (i.e. 90^{th} percentiles of model-based distributions) of NPCC2's SLR projections were derived for the 2050s (0.76 m) and 2080s (1.47 m), relative to the 1971-2000 baseline.

2.1.3 Topography dataset

Floodplain topography is available for NYC in the form of a Digital Elevation Model (DEM). The data were acquired by the NYC Department of Environmental Protection and the Department of Information Technology & Telecommunications in 2012 using Light Detection and Ranging (LiDAR) technology. The DEM was constructed from LiDAR point cloud with a horizontal resolution of 30 cm and a vertical accuracy of ± 10~20 cm. In this study, a "bare earth" topography based on North American Vertical Datum of 1988 (NAVD 88) was produced by removing non-topographic features (e.g. trees, cars and buildings). Building representation in urban hydrodynamic model is an active research field as buildings represent barriers to flow and reduce the area available for water storage (e.g. Yu and Lane 2006b; Fewtrell et al 2008; Neal e al. 2011). The impact of four treatment methods for building topography (building resistance, building block, building hole, and building porosity) has been investigated using a 2D flood inundation model (Schubert and Sanders, 2012). Results suggest that all four approaches support sufficiently accurate flood extent and stream flow prediction. The best method for a particular application depends on data availability, modeling objectives and user tolerances for pre-processing and run-time costs. Considering the size of the simulation domain and focus of the paper, building effects were modeled in our analysis using building resistance method, i.e. relatively high Manning coefficient. To reduce the computational costs, the 0.3 m LiDAR DEM was further resampled to a 6 m grid resolution using bilinear interpolation method, resulting in a DEM sufficiently fine to represent primary urban surface features (e.g. roads). Consequently, the simulation domain of the Lower Manhattan consists of 1000 × 1300 grids, or 1.3 million cells.

2.1.4 Road network and facilities

The most recent (updated in August 2016) GIS dataset of city facilities and a single line street base map (i.e. LION) were obtained from the NYC Open Data Portal[2]. Locations of critical emergency responders were identified from the city facility layer, including 30 fire houses (FS), 11 police stations (PS), and 2 EMS centers. Locations of vulnerable healthcare facilities include nursing homes, hospitals, hospices, and adult day care facilities were also derived from the dataset. City streets and traffic directions were extracted from LION. Current speed limits (i.e. 40 mph for F.D.R. (Franklin D. Roosevelt East River Drive), 35 mph for West Street, 11 and 12 Avenue, and 20~25 mph for the other roadways) were collected and assigned to each road sections in Lower Manhattan. Traffic signals and other driving regulations, which emergency vehicles are exempt from (e.g. one way and U-turn), were not considered. A transport network dataset was then created using the default turn restrictions in ArcGIS10.2.

2.2 Coastal flood modeling

A simplified 2D flood inundation model (FloodMap-Inertial) – a revised version of an earlier diffusion-based model (FloodMap, Yu and Lane 2006a, b) – was used to simulate the hydrodynamics of coastal flooding. The model has been calibrated for the NYC using the 2012 Hurricane Sandy event, against the highest water levels obtained from USGS HWMs (High Water Marks), deployed along the NYC coast prior to storm landfall. (Yin et al., 2016b). The simplified 2D solutions have been shown to perform as well as full 2D models for the treatment of coastal flooding, but at much lower computational cost (Bates et al., 2005). The module used here solves the inertial form of the 2D shallow water equations in a raster-based environment. Surface flood routing takes the same form as the inertial

[2] http://www1.nyc.gov/site/planning/data-maps/open-data.page

algorithm of Bates et al. (2010), but with a different approach to time step calculation, which forward calculates the optimal time step for the next iteration rather than using the time step calculated in the current iteration for the next. The details of the model structure have been presented in Yu and Lane (2011), and the key features of the model structure are presented below. The momentum equation in the Saint-Venant equations without the convective acceleration term takes the form:

$$\frac{\partial q}{\partial t} + \frac{gh\partial(h+z)}{\partial x} + \frac{gn^2q^2}{R^{4/3}h} = 0$$

where q is the flow per unit width, g is the acceleration due to gravity, R is the hydraulic radius, z is the bed elevation, h is the water depth, and n is the Manning's roughness coefficient. R can be approximated with h for wide and shallow flows. Discretizing the equation with respect to time gives:

$$\frac{q_{t+\Delta t} - q_t}{\Delta t} + \frac{gh_t\partial(h+z)}{\partial x} + \frac{gn^2q_t^2}{h_t^{7/3}} = 0$$

where one of the q_t in the friction term can be replaced by $q_{t+\Delta t}$, resulting in the explicit expression of the flow at the next time step:

$$q_{t+\Delta t} = \frac{q_t - gh_t\Delta t(\frac{\partial(h_t+z)}{\partial x})}{(1+gh_t\Delta t n^2 q_t / h_t^{10/3})}$$

Flows in the x and y directions are decoupled and take the same form. Discharge is evaluated at cell edges and depth at the cell centre. To maintain model stability and minimize numerical diffusion, the Forward Courant-Freidrich-Levy Condition (FCFL) approach described in Yu and Lane (2011) for the diffusion-based version of FloodMap is used in the inertial model to calculate the time step:

$$\Delta t <= \min(\frac{wd_id_jn}{d_i^{1.67}(S_i)^{1/2} + d_j^{1.67}(S_j)^{1/2}})$$

where w is the cell size, d_i and d_j are the effective water depths; S_i and S_j are water surface slopes; and i and j are the indices for the flow direction in the x and y directions, respectively. The effective water depth is defined as the difference between the higher water surface elevation and the higher bed elevation of two cells that exchange water. The minimum time step that satisfies the FCFL condition for all wet cells is used as the global time step for this iteration. This approach does not require the back calculation of Courant number as the time step is calculated based on the CFL condition that satisfies every wet grid cell for the current iteration. The universal time step calculated with FCFL may need to be scaled further by a coefficient, with a value between 0 and 1, as the FCFL condition is not strictly the right stability criteria for an inertial system. A scaling factor in the region 0.5 to 0.8 was found to yield a stable solution in previous studies – a scaling factor of 0.7 was used herein for all simulation. Calibration and validation of the model have been conducted for the study area in Yin et al. (2016b). A relatively high floodplain roughness value (Manning's n=0.06) was used in the present simulations to represent the effect of urban features (e.g. buildings) on flow routing.

To apply FloodMap for inundation simulation, we convert the static flood scenarios to dynamic boundary conditions, by scaling Hurricane Sandy's stage hydrograph. Specifically, the hourly water level recorded at the Battery gauge station during Hurricane Sandy was scaled according to each flood scenario. A constant tidal cycle with two rising phases and two falling limbs, similar to that during Hurricane Sandy, was applied. The stage hydrograph was scaled for and applied to each of the 23 coastline sections (defined by the FEMA flood maps) in the study area to drive the inundation analysis. The baseline 2012 tidal hydrograph was scaled up proportionally from the onset to the peak where the projected SLR heights are imposed.

2.3 Emergency response evaluation

2.3.1 Defining flood restriction

Regular vehicles such as compact or full size cars should avoid travelling through flood water higher that 25-35 cm as these are the heights of their exhaust pipes, water above which may cause loss of control for the moving vehicles. In many cities around the world (e.g. Shanghai), floodwater depth ⩾ 25 cm was adopted as a critical threshold for road closures. Previous studies in the UK (e.g. Green et al., 2017; Coles et al., 2017) used 25 cm as a threshold of blockage to emergency vehicles (Ambulance; Fire & Rescue), based on the understanding that the depth of extensive waterbody on the road may be difficult to determine any submerged objects or features (such as open manhole covers) that may pose unforeseen threats, even to emergency vehicles. Moreover, floodwater velocity is known to affect road infrastructures and vehicles (Kreibich et al., 2009). For example, Tingsanchali (1996) indicated that if the floodwater reaches an average depth of 0.5 m, a flow velocity of 1.0 m/s is the tipping point for vehicle instability. In case of higher velocity, a very shallow depth of water may raise at the contact of the vehicle, leading to unsafe wading (1.0 to 2.0 m/s) and even damage to light structures (over 2.0 m/s). According to NYC flood insurance study (2013), mean flood velocities in Manhattan are mostly less than 2.0 m/s. Emergency responders in the NYC are equipped with larger vehicles such as emergency heavy trucks which have a higher tolerance to traversing flood water. Therefore, instead of using the 25 cm depth threshold used in two previous studies (Coles et al. 2017; Green et al. 2017), we applied a 50 cm threshold as flood restrictions to emergency vehicles and flow velocity is considered in this case. Based on the coincidence of GIS roadways and water depths greater than 50 cm, street segments affected were determined and treated as barriers in the road network.

2.3.2 Emergency service analysis

Polygons were created to represent the service areas that can be reached from the emergency facilities within a given response time under normal (i.e. no flood) as well as disrupted conditions from different flood scenarios. The emergency service coverage was calculated based on the quickest routing weighted by travel time rather than the shortest path algorithm by distance from facility to destination. Using the facilities as starting points, travel impedance is set to use Drive Time (Minutes) in ArcGIS Network Analyst. Three service areas lying within a 3-min, 5-min and 8-min drive were specified for each facility, considering that different categories of incidents require different response timeframes. For example, records show that the travel time was on average about 3 ~ 5 minutes for high priority incidents in NYC during 2013 and 2016 (http://www.nyc.gov/html/911reporting/html/reports/end-to-end.shtml). In addition, taxi GPS data since 2010 show significant traffic congestion and temporal variation with an annual average travel speed of less than 10 mph in Lower Manhattan (NYC Department of Transportation, 2016). To account for the effect of traffic, the sensitivity of response time to congestion was evaluated by reducing the speed limits at a 5-mph interval (i.e. S1: speed limit, S2: speed limit minus 5mph, S3: speed limit minus 10mph and S4: speed limit minus 15mph). Total obstruction for a prolonged period of time is an unavoidable traffic condition in megacities, particularly in Lower Manhattan. In such situations, flood emergency response via road network would be completely interrupted. To consider such situations, traffic modelling is needed, and real-time traffic monitoring can provide live data for verifying and conditioning traffic modelling. This was not considered in our analysis.

3 Results and discussions

3.1 Coastal flood characteristics

Predicted maximum inundation depths for the 1 in 100- and 500-year coastal flood for the baseline, 2050s and 2080s scenarios are presented in Fig. 1. Comparison of the derived flood maps reveals three important findings. First, almost the entire waterfront area is subject to inundation during major flood scenarios at current and future states, due to a low-standard and fragmentary bulkhead coastal protection which is only 1.25 to 1.75 m above mean sea level in southern Manhattan (Colle et al. 2008). Second, coastal inundation extent increases proportionately with increased recurrence intervals and SLR projections over time. This can be largely attributed to the presence of lateral topographic confinement on the floodplain and thus flood water would be restricted to coastal low-lying regions, especially in the downtown area. Third, as expected, SLR significantly increases the maximum flood inundation. The magnitude of impacts, in terms of both extent and depth, depends on the rate of projected SLR. When the 0.76-m and 1.47-m rise in the local sea level for the 2050s and 2080s are considered, a 35 % and 60 % increase in total inundation area is observed for the 100-year flood scenarios and a 20% and 38% increase is observed for the 500-year flood scenarios.

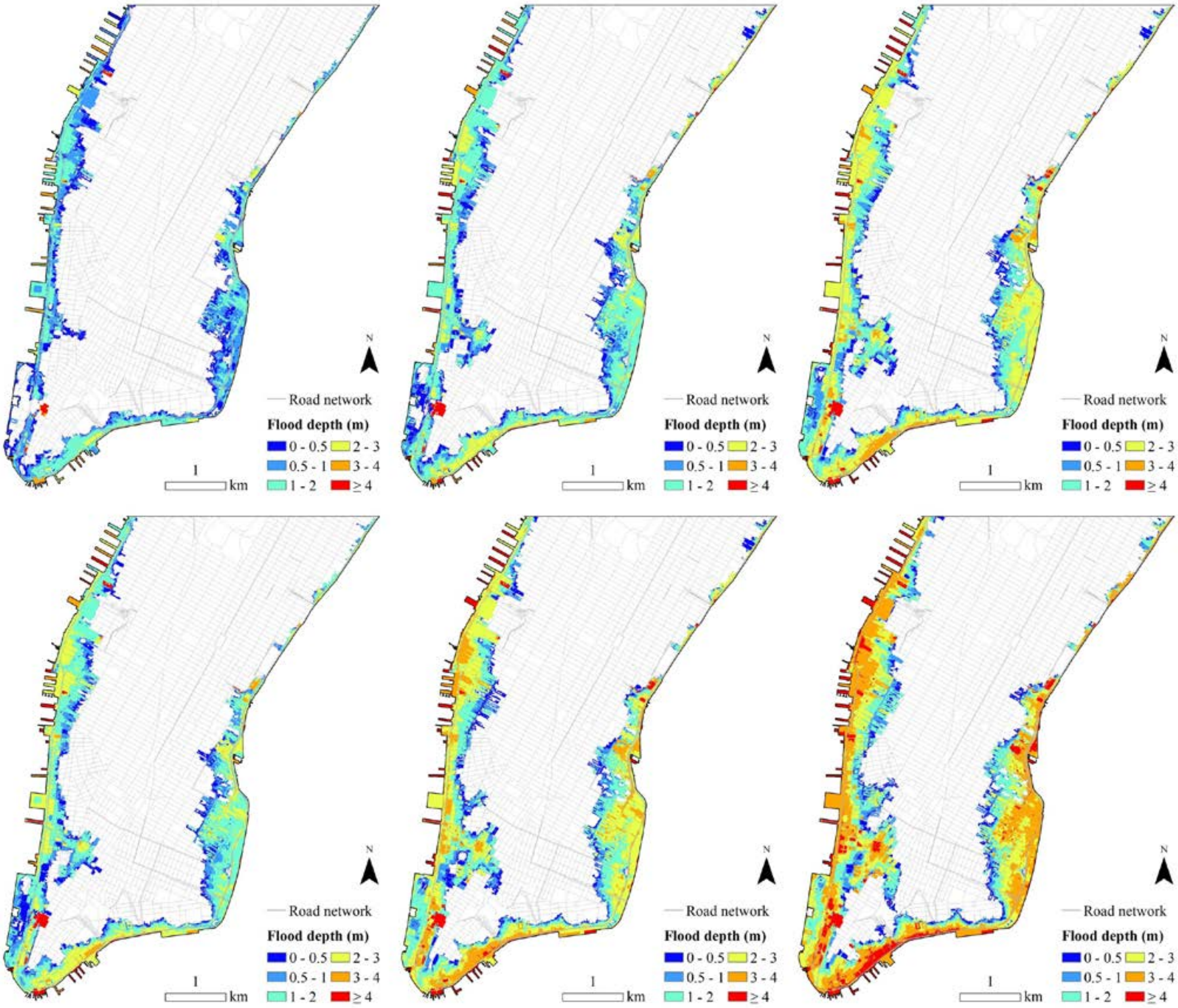

Fig. 1 Maximum inundation maps predicted by FloodMap for different scenarios: 100-year flood in 2012 (upper left), 100-year flood in 2050s (upper middle), 100-year flood in 2080s (upper right), 500-year flood in 2012 (lower left), 500-year

flood in 2050s (lower middle), 500-year flood in 2080s (lower right).

In order to illustrate the temporal characteristics of coastal flood dynamics, time series of inundation areas for each scenario are further explored and presented in Fig. 2. It is found that the corresponding time-area curves are in line with each other. This suggests that the timing of the inundated area is synchronized with the fluctuation of storm tide, expected of a relatively small domain with upward gradient further away from the shore. In each simulation, the inundated extent increases rapidly during the rising phase and maximum inundation is reached shortly after the flood peak, gradually decreasing afterwards as the stage subsides. Moreover, results indicate that SLR leads to proportionately larger impacts on coastal flooding throughout the simulations, confirming what is found in Fig. 1. With rapid rise in sea level, severe coastal inundation would occur more extensively in the low-lying floodplain, and for longer durations.

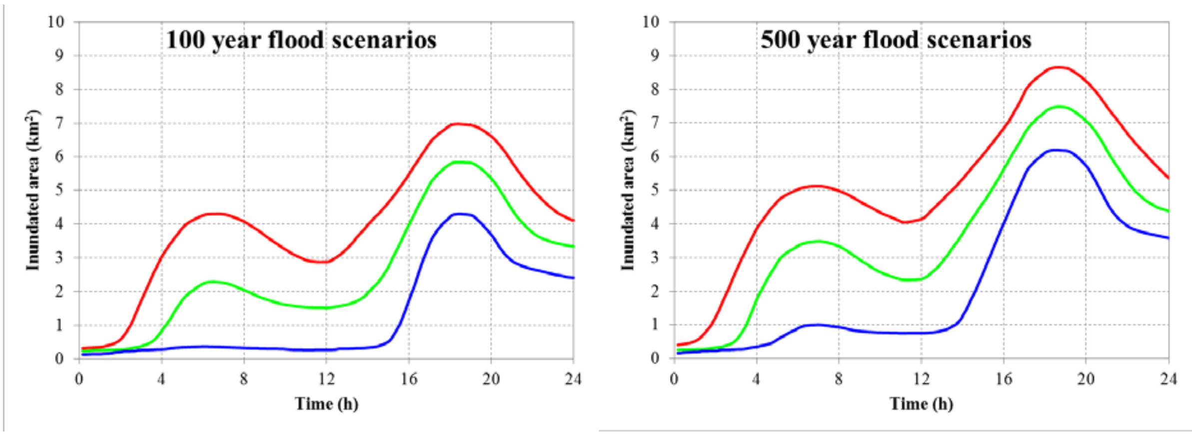

Fig. 2 Time series of inundation areas for 100- and 500-year flood scenarios in 2012 (blue line), 2050s (green line) and 2080s (red line).

3.2 Emergency response impacts

3.2.1 Emergency services under normal conditions

Network analysis under normal conditions shows that, when no flood restrictions are in place, almost the entire area is accessible within 8 minutes or less for fire and police services (Fig. 3 and Table 1). The sensitivity analysis of travel speeds further reveals that fire and police emergency responses would be able to reach the majority of Lower Manhattan within 3 minutes or 5 minutes even under adverse traffic conditions. For example, if emergency vehicles drive at speed S4 (i.e. speed limit minus 15mph), 92% and 74% of the area would be covered within 5 minutes by the fire and police services respectively. The response times presented here match well with the observations which are about 3 to 5 minutes of average traveling for major FDNY (category-1, 2, 3 and 4) and NYPD (category-1 and 2) emergency incident[3]. In addition, significant areas can be served by multiple fire and police stations during emergency response. These findings suggest that fire houses and police stations are well placed throughout the region with sufficient overlaps in the service area of each facility, providing a good degree of contingencies for emergency response in situations where certain stations are out of action.

Table 1 Accessibility of emergency services with various travel speeds under non-flood conditions. Unit: km^2.

[3] http://www.nyc.gov/html/911reporting/html/reports/end-to-end.shtml

Emergency services	EMS with various travel speeds				FDNY with various travel speeds				NYPD with various travel speeds			
	S1	S2	S3	S4	S1	S2	S3	S4	S1	S2	S3	S4
Accessible in 3 minutes	6.9 (26%)	4.25 (16%)	2.33 (9%)	1.06 (4%)	24.55 (94%)	24.41 (94%)	22.68 (87%)	14.79 (57%)	24.11 (93%)	22.58 (87%)	16.49 (63%)	7.03 (27%)
Accessible in 5 minutes	16.28 (63%)	11.59 (45%)	7.25 (28%)	3 (12%)	25 (96%)	24.95 (96%)	24.87 (96%)	23.92 (92%)	24.95 (96%)	24.88 (96%)	24.65 (95%)	19.31 (74%)
Accessible in 8 minutes	25.31 (97%)	22.32 (86%)	16.83 (65%)	9.47 (36%)	25.65 (99%)	25.65 (99%)	25.65 (99%)	25.65 (99%)	25.66 (99%)	25.65 (99%)	25.65 (99%)	25.61 (99%)

In terms of emergency medical services, the results indicate that, under no flood conditions, spatial coverage of EMS is sensitive to traffic conditions. This is due to the limited number of EMS centers and their uneven distribution (Fig. 3). In Lower Manhattan, there are only two EMS stations that are located in the southern- and mid-eastern parts of the city respectively. Compared to the fire and police services, significantly less coverage is predicted for EMS, especially within the 3- and 5-minute timeframes, with the northwest region most vulnerable. Although 97% of Lower Manhattan would be reachable within 8 minutes or less in unobstructed traffic conditions (e.g. in the evenings), the 8-min EMS response zones cover only 36% of the total area when significant congestion occurs (S4), reducing to 12% and 4% within 5-minute and 3-minute respectively. The results are consistent with the actual EMS response times which were on average 6.39 minutes for life threatening incidents and 9.04 minutes for non-life threatening incidents[4].

[4] http://www.nyc.gov/html/911reporting/html/reports/end-to-end.shtml

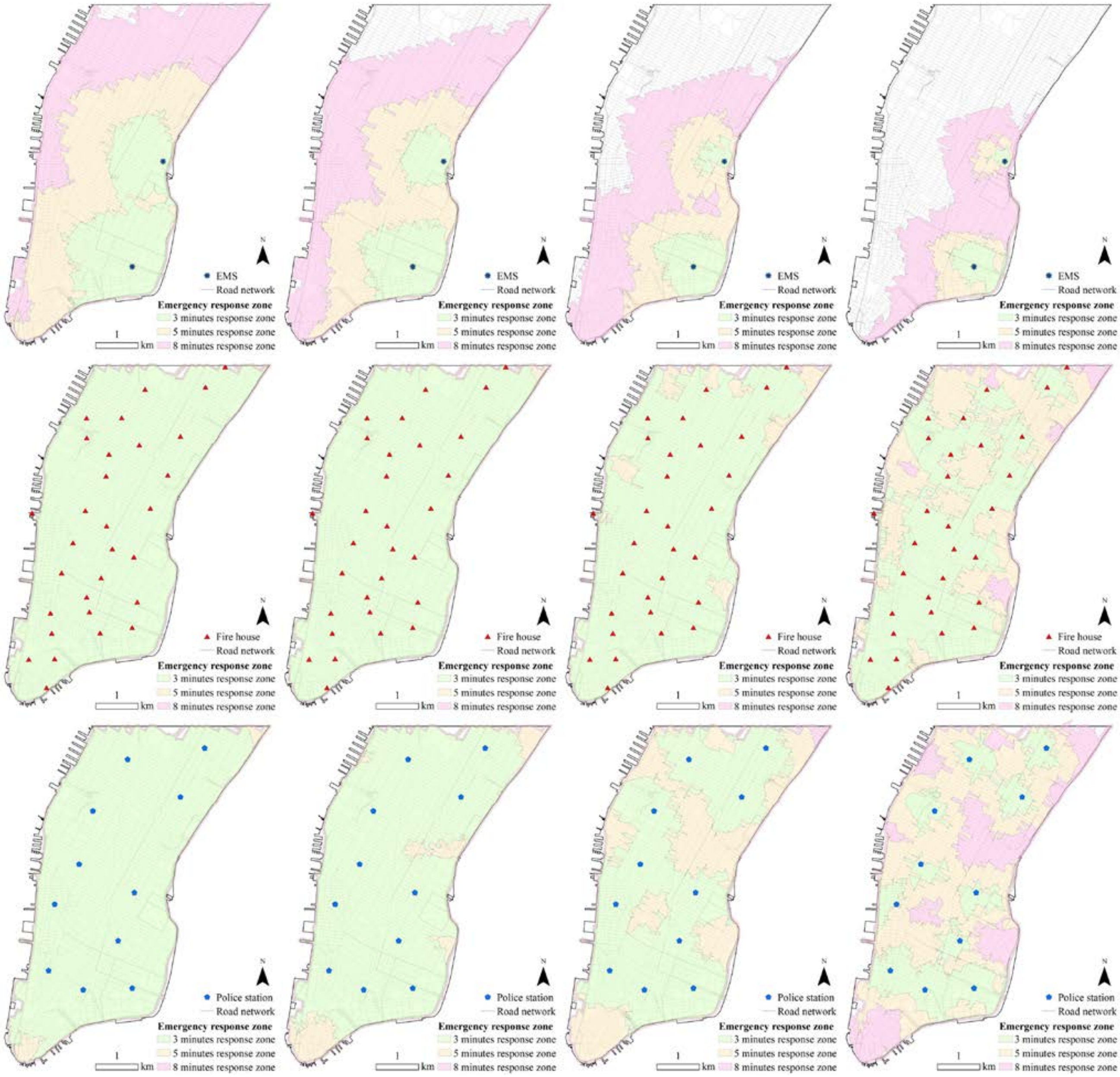

Fig. 3 Emergency service areas for (3 (green), 5 (yellow), and 8 (pink) -minute timeframes) EMS (upper), Fire houses (middle) and Police Stations (lower) under normal (no flood) conditions with different travel speeds: S1 in the first column for S1, S2 in the second column for S2, S3 in the third column for S3, and S4 in the fourth column for S4.

3.2.2 Emergency services under flood scenarios

When flood restrictions are incorporated into the network analysis, road disruptions and inaccessible areas can be identified for each scenario (Table 2). To illustrate such impacts, emergency service areas covered by 3-, 5- and 8-minute response times with S1 and S4 travel speeds under 100- and 500-year coastal flood scenarios are illustrated in Fig. 4. The results suggest that coastal flooding exerts varying degrees of impact on the three types of emergency response coverage. For fire and police services, emergency response can still reach the majority of the area where the road network has not been disrupted by coastal flooding. This is due to the significant overlaps between service areas of individual stations, which to a large extent compensate for losses in the coverage by stations directly affected by flooding. In contrast, because of the proximity to shoreline, floodwater directly compromises one of the two EMS centers in all scenarios, leading to a significant reduction (over 30% of the total area) in response coverage to the north of the region. Moreover, a notable 'blind spot' at the island's southern tip can be observed for ambulance and police services under the 2080s flood scenarios due to a lack of in-place facilities and key access routes under floodwater.

The simulations also show that emergency response service areas gradually decrease with increasing flood magnitude. Around 83% of the total area is reachable in 8 minutes or less by fire and police services under the current 100-year coastal flood event, compared to 75% under the current 500-year scenario. With a 0.76 m rise in sea level projected for 2050s, one police station and two to five fire houses would be directly affected, and 76% and 71% of the road network would be accessible within 8 minutes under 100- and 500-year flood scenarios. When compared with the normal operating conditions, a projected 1.47-m rise in sea level is expected to contribute a 28% to 33% reduction in accessible areas under 100- and 500-year scenarios in 2080s respectively. Up to 37% of Lower Manhattan would be entirely unreachable or 'islanded' for police emergency services under the 500-year scenario in the 2080s, indicating that SLR has significant and non-linear impacts on emergency response spatial accessibility.

For the ambulance emergency services, the impact of coastal inundation is more pronounced as only one EMS center would be operational in the flood scenarios. Additionally, the service area is highly sensitive to travel speeds of ambulance vehicles. For example, under normal traffic conditions (i.e. S1), over half (51%) of the area is predicted to be accessible within 8 minutes in the current 100-year flood scenario, compared to 46% under the current 500-year scenario. By contrast, only 15% and 14% of the community can be reached in 8 minutes in congested traffic conditions (i.e. S4) under current 100- and 500-year flood scenarios, respectively. The insensitivity of service to flood magnitude under the same traffic conditions can be explained by the overlaps of EMS spatial coverage between ambulance stations. Furthermore, the impact of SLR on EMS's spatial accessibility for both the 100- and 500-year events demonstrates similar patterns as the fire and police services, with slight decreases in the coverage from present day to 2050s to 2080s. SLR, coastal flood events and the operation of emergency service have different timescales. SLR evolves over decadal and centennial timescales and amplifies storm impact (i.e. duration and/or extent) during period of flood events (days, hours), whilst emergency service responds to coastal flood events that may last hours to days on demand. With the consideration of SLR into discrete points into the near future (2050 and 2080), we investigate how long-term evolution of SLR affects the event-scale emergency responses.

To investigate the relative impact of SLR on emergency response time, the ambulance response time to healthcare facilities is further quantified via fastest routing under normal and flood scenarios in Lower Manhattan (Fig. 5). Results suggest that compared to normal condition, coastal flooding causes significant increases in response times, mostly due to the lack of access from one EMS and the disruption of coastal highways (e.g. F.D.R). The modelled response time ranges from 0.33 to 8.18 min with an average value of 3.82 min in unobstructed traffic (i.e. S1) under no flood condition, while the average response time increases significantly to 6.18 and 6.19 minutes for the current 100y and 500y flood scenarios, respectively. However, SLR exerts a relatively minor impact on EMS response time. For example, with a 1.47 m rise in sea level, ambulance response time on average increases by 0.32 minute for a 500y flood event. This can be attributed to the confined nature of flood extents in coastal floodplains.

Table 2 Accessibility of emergency services with various travel speeds under flood scenarios in current state, 2050s and 2080s. Unit: km^2.

Responses with various travel speed	Accessible in current 100-flood scenario			Accessible in current 500-flood scenario			Accessible in 2050s 100-flood scenario			Accessible in 2050s 500-flood scenario			Accessible in 2080s 100-flood scenario			Accessible in 2080s 500-flood scenario		
	3min	5min	8min	3min	5min	8min	3min	5min	8min	3min	5min	8min	3min	5min	8min	3min	5min	8min
EMS-S1	3.19	7.52	13.35	2.83	6.58	11.87	2.86	6.73	12.11	2.66	5.75	11.09	2.71	6.07	11.3	2.48	4.49	9.05
	(12%)	(29%)	(51%)	(11%)	(25%)	(46%)	(11%)	(26%)	(47%)	(10%)	(22%)	(43%)	(10%)	(23%)	(43%)	(10%)	(17%)	(35%)
EMS-S2	2.15	5.43	10.74	1.95	4.62	9.55	1.96	4.69	9.77	1.85	4.28	8.76	1.88	4.41	8.95	1.75	3.52	6.94
	(8%)	(21%)	(41%)	(8%)	(18%)	(37%)	(8%)	(18%)	(38%)	(7%)	(16%)	(34%)	(7%)	(17%)	(34%)	(7%)	(14%)	(27%)
EMS-S3	1.33	3.35	7.71	1.23	2.93	6.78	1.23	2.96	6.95	1.17	2.76	6.01	1.19	2.79	6.28	1.08	2.56	4.68
	(5%)	(13%)	(30%)	(5%)	(11%)	(26%)	(5%)	(11%)	(27%)	(5%)	(11%)	(23%)	(5%)	(11%)	(24%)	(42%)	(10%)	(18%)
EMS-S4	0.65	1.65	4	0.62	1.5	3.52	0.63	1.53	3.6	0.58	1.43	3.3	0.58	1.46	3.39	0.53	1.33	3.06
	(3%)	(6%)	(15%)	(2%)	(6%)	(14%)	(2%)	(6%)	(14%)	(2%)	(6%)	(13%)	(2%)	(6%)	(13%)	(2%)	(5%)	(12%)
FDNY-S1	20.07	20.66	21.51	18.19	18.74	19.51	18.4	18.96	19.76	17.27	17.81	18.57	17.52	18.06	18.83	16.09	16.65	17.44
	(77%)	(79%)	(83%)	(70%)	(72%)	(75%)	(71%)	(73%)	(76%)	(66%)	(69%)	(71%)	(67%)	(69%)	(72%)	(62%)	(64%)	(67%)
FDNY-S2	19.87	20.61	21.51	18.08	18.68	19.5	18.3	18.91	19.75	17.15	17.76	18.57	17.4	18.01	18.82	15.97	16.61	17.45
	(76%)	(79%)	(83%)	(70%)	(72%)	(75%)	(70%)	(73%)	(76%)	(66%)	(68%)	(71%)	(67%)	(69%)	(72%)	(61%)	(64%)	(67%)
FDNY-S3	18.31	20.48	21.5	16.95	18.59	19.51	17.11	18.81	19.75	16.03	17.66	18.57	16.22	17.91	18.82	14.83	16.5	17.44
	(70%)	(79%)	(83%)	(65%)	(72%)	(75%)	(66%)	(72%)	(76%)	(62%)	(68%)	(71%)	(62%)	(69%)	(72%)	(57%)	(63%)	(67%)
FDNY-S4	12.05	19.41	21.51	11.2	17.9	19.5	11.34	18.07	19.75	10.56	16.95	18.57	10.71	17.18	18.82	9.56	15.75	17.45
	(46%)	(75%)	(83%)	(43%)	(69%)	(75%)	(44%)	(70%)	(76%)	(41%)	(65%)	(71%)	(41%)	(66%)	(72%)	(37%)	(61%)	(67%)
NYPD-S1	19.77	20.59	21.5	17.85	18.66	19.5	18.17	18.9	19.76	16.98	17.73	18.58	17.29	17.99	18.83	15.2	15.76	16.46
	(76%)	(79%)	(83%)	(69%)	(72%)	(75%)	(70%)	(73%)	(76%)	(65%)	(68%)	(71%)	(67%)	(69%)	(72%)	(58%)	(61%)	(63%)
NYPD-S2	18.87	20.49	21.5	17.06	18.57	19.5	17.35	18.81	19.75	16.06	17.64	18.58	16.41	17.91	18.84	14.59	15.69	16.45
	(73%)	(79%)	(83%)	(66%)	(71%)	(75%)	(67%)	(72%)	(76%)	(62%)	(68%)	(71%)	(63%)	(69%)	(72%)	(56%)	(60%)	(63%)
NYPD-S3	14.27	20.11	21.5	12.76	18.27	19.59	12.9	18.51	19.75	11.96	17.3	18.58	12.03	17.61	18.84	10.9	15.52	16.49
	(55%)	(77%)	(83%)	(49%)	(70%)	(75%)	(50%)	(71%)	(76%)	(46%)	(67%)	(71%)	(46%)	(68%)	(72%)	(42%)	(60%)	(63%)
NYPD-S4	6.29	16.36	21.29	5.45	14.69	19.23	5.71	14.89	19.67	5.11	13.79	18.36	5.12	13.92	18.66	4.79	12.69	16.39
	(24%)	(63%)	(82%)	(21%)	(57%)	(74%)	(22%)	(57%)	(76%)	(20%)	(53%)	(71%)	(20%)	(54%)	(72%)	(18%)	(49%)	(63%)

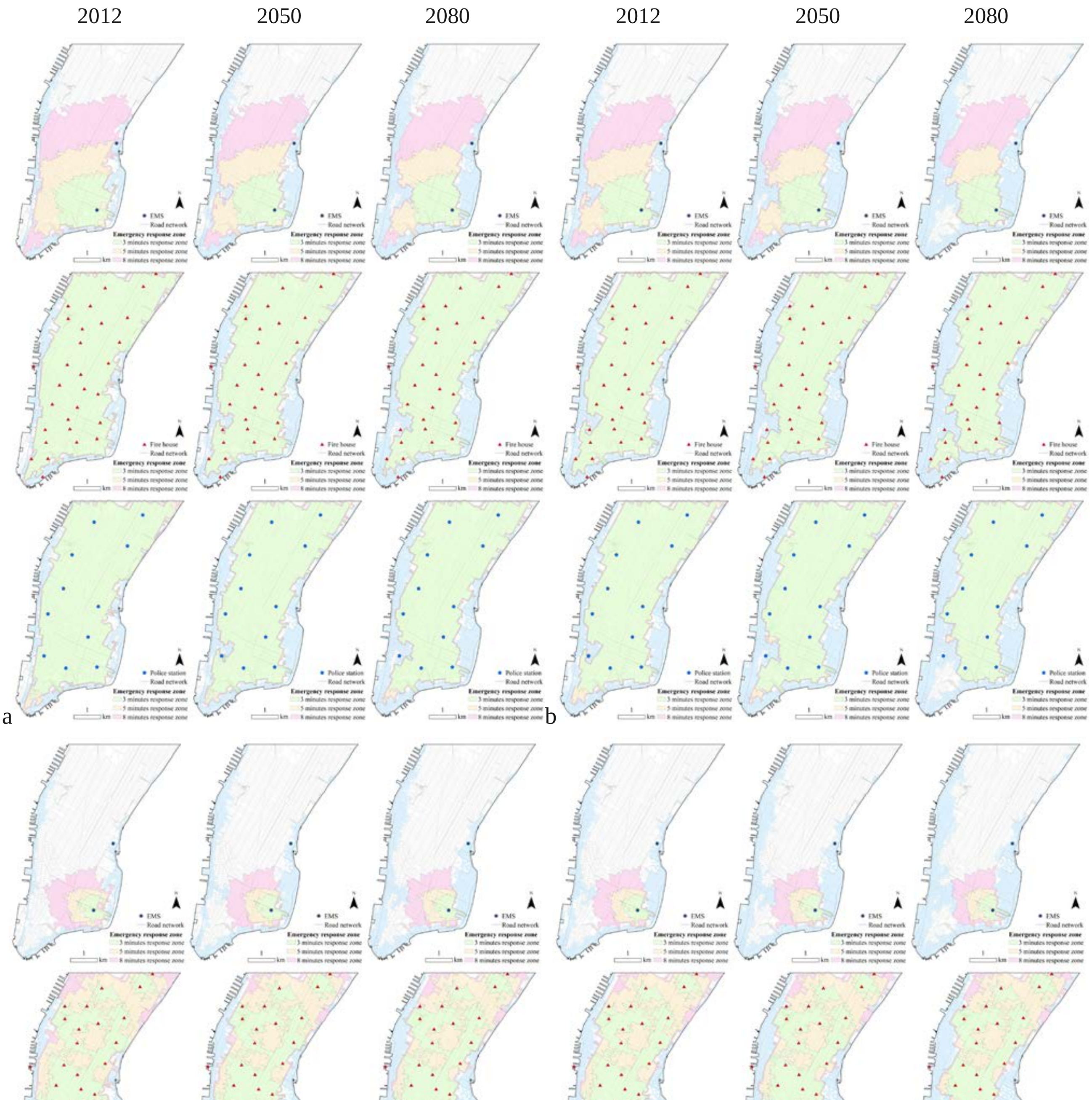

Fig. 4 Emergency service areas in 3-, 5- and 8-minute response timeframes for EMS, fire houses and police stations under various SLR and coastal flood conditions and different travel speeds: (a) 100-year flood scenarios with S1; (b) 500-year flood scenarios with S1; (c) 100-year flood scenarios with S4; (d) 500-year flood scenarios with S4. Light blue represents

water depth higher than 50 cm.

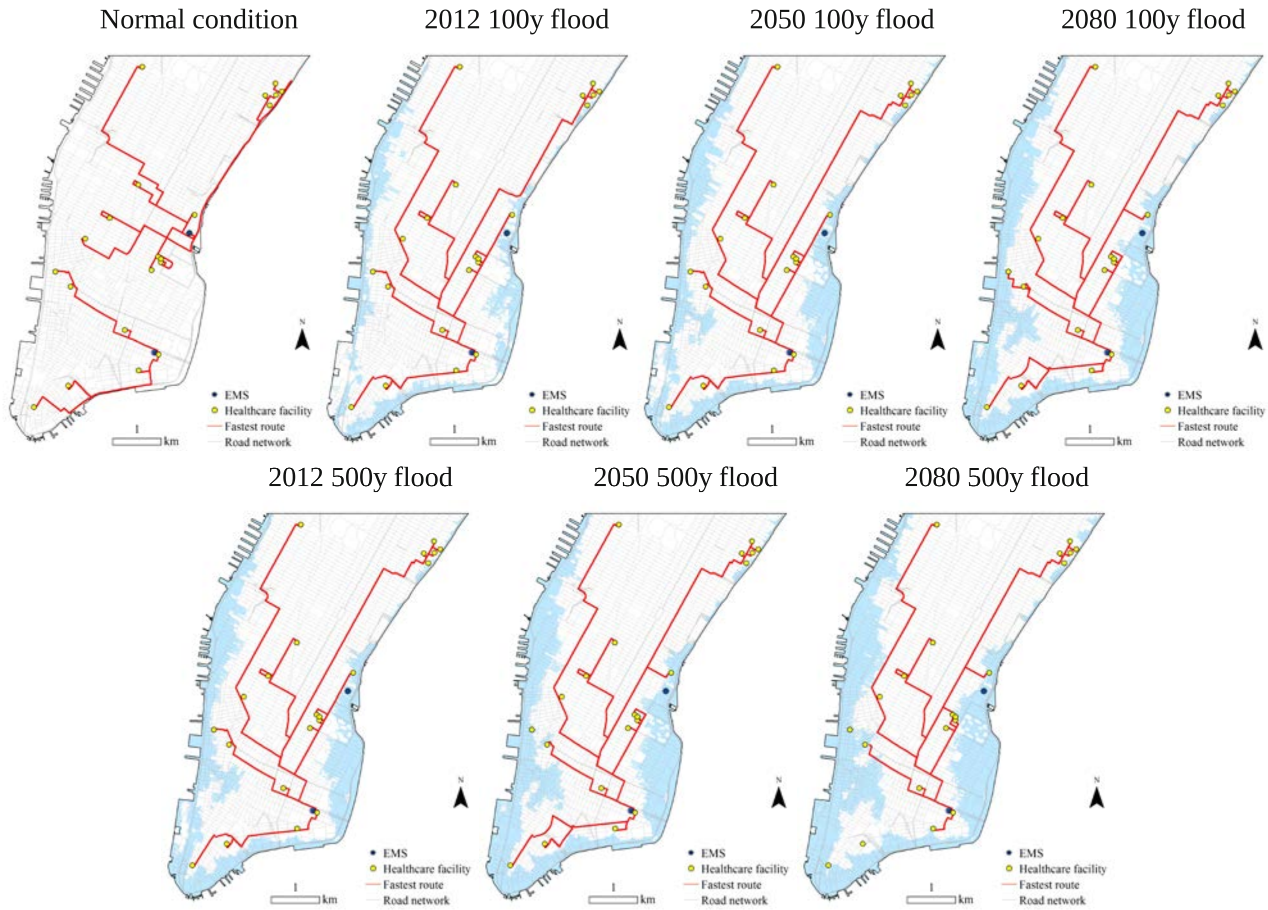

Fig. 5 Fastest routes between EMS and healthcare facilities in Lower Manhattan at normal and coastal flood conditions

3.3 Future perspective and adaptation measures

Since Lower Manhattan is physically and socio-economically vulnerable to the impacts of SLR and coastal flood events, appropriate resilience measures should be implemented to mitigate the potential negative consequences. As the most effective measure, a coastal flood protective system (BIG U) is likely to be initiated in the next few years to protect the city against SLR and Sandy-like stormwater in the future (Rosenzweig and Solecki, 2014). The project will loop around the entire shoreline of Lower Manhattan with 10 continuous miles of reinforced seawall, stretching from West 57th street south to the Battery and up to East 42th street. The coastal flood defence is designed to withstand a present-day one in 100-year flood plus NPCC's 2050s high-end SLR projection. With this major flood defence system in place, future flood risk and associated impact on emergency responses in the short- to medium-term are expected to be alleviated for this part of the city. However, low probability flood events (i.e. 1 in 100- and 1 in 500-year events) may still pose threats to the city over the long term (e.g. 2080s). Hence a new set of approaches (i.e. adaptation pathways) are required to develop sustainable policies and planning which can address the uncertainties from long term change and support flexibility in systems design and management (Deng et al., 2013; Buurman and Babovic, 2016; Manocha and Babovic, 2017).

In addition to directly tackling SLR and flood hazards, alternative measures can be adopted by emergency services. For example, availability of waterproof vehicles and maneuverable boats which can be easily carried and deployed for storage on a vehicle during coastal flood rescue operations could be one option. Furthermore, emergency service stations could be more strategically positioned to minimize response travel time and maximize spatial coverage with optimal overlap. For example, the EMS center situated in coastal floodplain could be relocated to the middle or north of the region. We also suggest that prepositioning 'stand-by' vehicles in predicted 'blind spots' as well as establishing temporary facilities (e.g. mobile pumping, demountable floodwall and inflatable bags) at critical nodes or linkages before potential flooding could significantly reduce disruption to emergency services. Moreover, prioritizing the evacuation of vulnerable people (e.g. homebound and elderly residents) and facilities (hospitals and nursing homes) in flood-prone areas would significantly lessen the burden of emergency response during and after a catastrophic flood event.

4 Conclusions

This study integrated a high resolution 2D hydraulic model (FloodMap) and a widely used GIS spatial analysis tool (Network Analyst) in order to evaluate SLR and coastal flood impacts on emergency service accessibility in Lower Manhattan, NYC. A number of conclusions can be drawn. First, coastal flooding combined with SLR is likely to reduce emergency response spatial coverage and response time via disruption to road network. Second, the performance of emergency services also depends on the station positioning and traffic conditions under both normal and flood scenarios. Finally, even with anticipated strengthening of coastal flood defences in the near future, emergency responders should still be prepared for a potential extreme flood event in a fast changing and uncertain climate. The approach presented here can be readily adopted for applications in other mega- coastal cities such as Shanghai, Mumbai, Bangkok and Jakarta which are particularly vulnerable to SLR and coastal flooding. However, data may not be readily available for developing nations, in particular the integrated transport network (ITN). Methods that adopt simplified ITN in their analysis should be developed for applications in data-sparse situations.

The analysis provides a detailed analysis of emergency service vulnerability to SLR and coastal flooding, and thus helps to guide decision-making for sustainable coastal flood emergency planning and management. However, to gain more insight and arrive at more robust conclusions, further research is warranted for the following aspects: (i) evaluating the duration, in addition to the spatial coverage of loss of accessibility for emergency services; (ii) incorporating traffic modeling into emergency response assessment to generate more reliable (variable) travel speeds and response times under different scenarios; and (iii) more sophisticated evaluation of network disruption that could take into account velocities as well as depths, and/or severe impedance by debris even in relatively shallow flood waters; and (iv) developing capabilities to forecast accessibility ahead of, during and in the aftermath of coastal flood events to guide operational responses in real-time. Moreover, the present analysis focuses on above ground emergencies, future studies should also be undertaken to assess response times and access to emergencies in flood/partially flooded subways, basements and underground car parks.

Acknowledgments This paper was supported by the National Science Foundation of the United States (Grant no: EAR-1520683), the National Natural Science Foundation of China (Grant no: 41201550) and the Humanities and Social Science Project of Education Ministry of China (Grant no: 17YJAZH111). This research extended work supported by the UK Natural Environment Research Council under the Environmental Risks to Infrastructure Innovation Programme (NE/M008770/1; NE/N013050/1; NE/R009600/1).

References

Aerts J C, Botzen W J, Emanuel K, Lin N, de Moel H, Michel-Kerjan E O, 2014. Evaluating flood resilience strategies for

coastal mega-cities. Science, 344: 473-475.
Bates P D, Dawson R J, Hall J W, Horritt M S, Nicholls R J, Wicks J, Hassan M A A M, 2005. Simplified two-dimensional numerical modelling of coastal flooding and example applications. Coastal Engineering, 52: 793-810.
Bates P D, Horritt M, Fewtrell T, 2010. A simple inertial formulation of the shallow water equations for efficient two-dimensional flood inundation modelling. Journal of Hydrology, 387: 33-45.
Blumberg A, Georgas N, Yin L, Herrington T, Orton P, 2015. Street Scale Modeling of Storm Surge Inundation along the New Jersey Hudson River Waterfront. Journal of Atmospheric and Oceanic Technology, doi:10.1175/JTECH-D-14-00213.1.
Buurman J, Babovic V, 2016. Adaptation Pathways and Real Options Analysis: An approach to deep uncertainty in climate change adaptation policies. Policy and Society, 35 (2): 137-150.
Chang H, Lafrenz M, Jung I, Figliozzi M, Platman D, Pederson C, 2010. Potential impacts of climate change on flood-induced travel disruptions: a case study of Portland, Oregon, USA. Annals of the Association of American Geographers, 100: 1-14.
Coles D, Yu D, Wilby R L, Green D, Herring Z, 2017. Modelling emergency service accessibility during flooding in York, UK, Journal of Hydrology, 546: 419-436.
Colle B A, Buonaiuto F, Bowman M J, Wilson R E, Flood R, Hunter R, Mintz A, Hill D, 2008. New York City's vulnerability to coastal flooding. Bulletin of the American Meteorological Society, 89: 829-841.
Deng Y, Cardin M, Babovic V, Santhanakrishnan D, Schmitter P, Meshgi A, 2013. Valuing flexibilities in the design of urban water management systems. Water research, 47 (20): 7162-7174.
Fewtrell T, Bates P D, Horritt M, Hunter N, 2008. Evaluating the effect of scale in flood inundation modelling in urban environments. Hydrological Processes, 22: 5107-5118.
Engelhart S E, Horton B P, 2012. Holocene sea level database for the Atlantic coast of the United States. Quaternary Science Reviews, 54: 12-25.
Federal Emergency Management Agency, 2013. Flood insurance study: City of New York.
Gil J, Steinbach P, 2008. From flood risk to indirect flood impact: evaluation of street network performance for effective management, response and repair. in Proverbs D, Brebbia C A, Penning-Roswell E (eds.) Flood Recovery, Innovation and Response (FRIAR 2008), Wessex Institute of Technology Press, UK, 335-345.
Green, D., Yu, D., Pattison, I., Wilby, R., Bosher, L., Patel, R., Thompson, P., Trowell, K., Draycon, J., Halse, M., Yang, L., and Ryley, T. (2017). City-scale accessibility of emergency responders operating during flood events, Nat. Hazards Earth Syst. Sci., 17, 1-16, doi:10.5194/nhess-17-1-2017.
Hallegatte S, Green C, Nicholls R J, Corfee-Morlot J, 2013. Future flood losses in major coastal cities. Nature Climate Change, 3: 802-806.
Hay C C, Morrow E, Kopp R E, Mitrovica J X, 2015.Probabilistic reanalysis of twentieth-century sea-level rise. Nature, 517: 481-484.
Horton R, Little C, Gornitz V, Bader D, Oppenheimer M, 2015. New York City Panel on Climate Change 2015 Report Chapter 2: Sea Level Rise and Coastal Storms. Annals of the New York Academy of Sciences, 1336: 36-44.
Hu A, Deser C, 2012. Uncertainty in future regional sea level rise due to internal climate variability. Geophysical Research Letters, 40: 2768-2772.
IPCC, 2012. Climate Change 2012: The Physical Science Basis. Cambridge University Press, Cambridge.
Kopp R E, Horton R M, Little C M, Mitrovica J X, Oppenheimer M, Rasmussen D J, Strauss B H, Tebaldi C, 2014. Probabilistic 21st and 22nd century sea level projections at a global network of tide gauge sites. Earth's Future, 2: 383-406.
Kreibich H, Piroth K, Seifert I, Maiwald H, Kunert U, Schwarz J, Merz B, Thieken A H, 2009. Is flow velocity a significant parameter in flood damage modelling? Natural Hazards and Earth System Sciences, 9: 1679-1692.

Levermann A, Griesel A, Hofmann M, Montoya M, Rahmstorf S, 2005. Dynamic sea level changes following changes in the thermohaline circulation. Climate Dynamics, 24(4): 347–354.

Manocha N, Babovic V, 2017. Development and valuation of adaptation pathways for storm water management infrastructure, Environmental Science & Policy, 77: 86-97.

Mitrovica J X, Tamisiea M E, Davis J L, Milne G A, 2001. Recent mass balance of polar ice sheets inferred from patterns of global sea-level change. Nature, 409: 1026-1029.

Neal J C, Schumann G, Fewtrell T, Budimir M, Bates P, Mason D, 2011. Evaluating a new LISFLOOD-FP formulation using data for the summer 2007 floods in Tewkesbury, UK. Journal of Flood Risk Management, 4(2): 88-95.

Nicholls R J, Cazenave A, 2010. Sea-level rise and is impacts on coastal zones. Science, 328: 1517–1520.

Lin N, Emanuel K Oppenheimer M, Vanmarcke E, 2012. Physically based assessment of hurricane surge threat under climate change. Nature Climate Change, 2(6): 462-467.

Lin N, Kopp R E, Horton B P, Donnelly J P, 2016. Hurricane Sandy's flood frequency increasing from year 1800 to 2100. Proceedings of the National Academy of Sciences, doi: 10.1073/pnas.1604386113.

NYC Department of Transportation, 2016. 2016 New York City Mobility Report. New York City, NY, USA.

NPCC2 Climate Risk Information, 2013. Climate Methods Memorandum. New York City Council, Available at: http://www.nyc.gov/html/planyc2030/downloads/pdf/NPCC2_Climate%20Methods%20Memorandum_2013.pdf?epi-content=GENERIC

NYC Mayor's Office, 2012. NYC Hurricane Sandy After Action: Report and Recommendations to Mayor Michael R. Bloomberg. New York City, NY, USA.

NYC Office of Emergency Management, 2014. 2014 New York City Hazard Mitigation Plan. New York City, NY, USA.

Peltier W R, 2004. Global glacial isostasy and the surface of the ice-age Earth: The ICE-5G (VM2) model and GRACE. Annual Review of Earth and Planetary Sciences, 32: 111-149.

Ramirez J A, Lichter M, Coulthard T J, Skinner C, 2016. Hyper-resolution mapping of regional storm surge and tide flooding: comparison of static and dynamic models. Natural Hazards, doi:10.1007/s11069-016-2198-z.

Rosenzweig C, Solecki W, 2014. Hurricane Sandy and adaptation pathways in New York: Lessons from a first-responder city. Global Environmental Change, 28: 395-408.

Schubert J E, Sanders B F, 2012. Building treatments for urban flood inundation models and implications for predictive skill and modeling efficiency. Advances in Water Resources, 41: 49-64.

Talke S A, Orton P, Jay D A, 2014. Increasing storm tides at New York City, 1844-2012. Geophysical Research Letters, 41: 3149-3155.

Tingsanchali T, 1996. Floods and human interaction: experiences, problems, and solutions, report. Asian Institute of Technology, Bangkok, Thailand.

Wang H V, Loftis J D, Liu Z, Forrest D, Zhang J, 2014. The Storm Surge and Sub-Grid Inundation Modeling in New York City during Hurricane Sandy. Journal of Marine Science and Engineering, 2: 226-246.

Yin J, Yu D, Yin Z, Liu M, He Q, 2016. Evaluating the impact and risk of pluvial flash flood on intra-urban road network: a case study in the city center of Shanghai, China. Journal of Hydrology, 537: 138-145.

Yin J, Lin N, Yu D, 2016. Coupled modeling of storm surge and coastal inundation: a case study in New York City during Hurricane Sandy. Water Resources Research 52: 8685-8699.

Yu D, Lane S N, 2006a. Urban fluvial flood modelling using a two-dimensional diffusion wave treatment, part 1: mesh resolution effects. Hydrological Processes, 20: 1541-1565.

Yu D, Lane S N, 2006b. Urban fluvial flood modelling using a two-dimensional diffusion wave treatment, part 2: development of a sub grid-scale treatment. Hydrological Processes, 20: 1567-1583.

Yu D, Lane S N, 2011. Interaction between subgrid-scale resolution, feature representation and grid-scale resolution in flood inundation modelling. Hydrological Processes, 25: 36-53.